Eur. Phys. J. A (2017) **53**: 146
DOI 10.1140/epja/i2017-12339-9

THE EUROPEAN PHYSICAL JOURNAL A

Regular Article – Theoretical Physics

Search for α + core states in even-even Cr isotopes

M.A. Souza[1,2,a] and H. Miyake[1,b]

[1] Instituto de Física, Universidade de São Paulo, Rua do Matão, 1371, CEP 05508-090, Cidade Universitária, São Paulo - SP, Brazil
[2] Departamento de Mecânica, Instituto Federal de Educação, Ciência e Tecnologia de São Paulo - Campus São Paulo, Rua Pedro Vicente, 625, CEP 01109-010, Canindé, São Paulo - SP, Brazil

Received: 13 March 2017 / Revised: 25 May 2017
Published online: 13 July 2017 –
Communicated by T. Duguet

Abstract. The α + core structure is investigated in even-even Cr isotopes from the viewpoint of the local potential model. The comparison of Q_α/A values for even-even Cr isotopes and even-even $A = 46, 54, 56, 58$ isobars indicates that ^{46}Cr and ^{54}Cr are the most favorable even-even Cr isotopes for the α + core configuration. The ground state bands of the two Cr isotopes are calculated through a local α + core potential containing a nuclear term with (1 + Gaussian) × (W.S. + W.S.^{3}) shape. The calculated spectra give a very good description of most experimental ^{46}Cr and ^{54}Cr levels, including the 0^+ bandheads. The reduced α-widths, rms intercluster separations and $B(E2)$ transition rates are determined for the ground state bands. The calculations reproduce the order of magnitude of the available experimental $B(E2)$ values without using effective charges, indicate that the low-spin members of the ground state bands present a stronger α-cluster character, and point out that the ^{46}Cr ground state band has a significant degree of α-clustering in comparison with ^{44}Ti. The volume integral per nucleon pair and rms radius obtained for the α + ^{50}Ti potential are consistent with those reported previously in the analysis of α elastic scattering on ^{50}Ti.

1 Introduction

The α-cluster structure is present in nuclei of different mass regions and is matter of discussions with many different approaches. A comprehensive review of this research theme, as well as the nuclear clustering in general, is found in ref. [1], and recent advances are described in refs. [1,2]. The α-cluster model has been successful in describing energy levels, α-decay widths, electromagnetic transition strengths and α-particle elastic scattering data. Previous studies [3,4] have questioned whether the most likely cluster + core structures are determined strictly by the doubly closed shell for cluster and core. Our recent article [5] shows that the local potential model (LPM) with the α + core interpretation can be applied systematically in intermediate mass nuclei around the double shell closure at ^{90}Zr, obtaining a good description of the energy levels and orders of magnitude of the $B(E2)$ transition rates without the use of effective charges. Additionally, ref. [5] shows that the α + core potentials employed in ^{94}Mo and ^{96}Ru are similar to the real parts of the optical potentials used in other studies for the analyses of α + ^{90}Zr ($E_{\alpha,\mathrm{lab}} = 31.0$–$141.7$ MeV) and α + ^{92}Mo ($E_{\mathrm{c.m.}} \approx 13$–$19$ MeV) elastic scattering, respectively.

In the fp-shell region, ^{44}Ti is one of the most studied nuclei with the α + core interpretation, since it has the configuration of α-particle plus ^{40}Ca doubly magic core. Works on the α + ^{40}Ca structure in ^{44}Ti (examples in refs. [6–11]) show good descriptions of the ground state band and $B(E2)$ transition rates. Neighboring nuclei as ^{43}Sc, ^{43}Ti, and others at the beginning of the fp-shell have been analyzed with the LPM [12,13], however, considering the effect of noncentral forces that arise with non-zero spin cores. The α+core structure in the fp-shell region has also been examined in nuclei as ^{42}Ca and ^{43}Sc from the viewpoint of the orthogonality condition model [14,15] and deformed-basis antisymmetrized molecular dynamics [16] with favorable results.

The motivation of this work is the investigation of the α+core structure in nuclei of the Cr isotopic chain, which is near the well-studied ^{44}Ti and presents even-even nuclei without the α + {doubly closed shell core} configuration. The structure of the Cr isotopes has been analyzed in previous studies with different approaches, which are discussed in the following paragraphs.

Some works investigate the Cr isotopes in terms of the shell-model and its variations. Recently, Togashi *et al.* [17] investigated natural and unnatural-parity states in neutron-rich Cr and Fe isotopes using large-scale shell-model calculations, describing and predicting the energy

[a] e-mail: marsouza@if.usp.br
[b] e-mail: miyake@if.usp.br

levels of both natural and unnatural-parity states up to the high-spin states in Cr and Fe isotopes with $N \leq 35$. Kaneko *et al.* [18] analyzed neutron-rich Cr isotopes by using the spherical shell model; the results give a good description of the known energy levels for the even-even $^{52-62}$Cr and odd-mass $^{53-59}$Cr nuclei, predict a lowering of excitation energies around neutron number $N = 40$, and provide a good reproduction of the experimental $B(E2; 2_1^+ \rightarrow 0_1^+)$ values for ^{52}Cr and ^{54}Cr by using effective charges $e_\pi = 1.5e$ and $e_\nu = 0.5e$. Kotila and Lenzi [19] study the development of collectivity along the Cr and Fe isotopic chains by using the interacting shell model and the proton-neutron interacting boson model; the two methods describe well the excitation energies of the yrast states in Cr isotopes, as well as the transition probabilities, and the ratios of the excitation energies $E_x(4_1^+)/E_x(2_1^+)$ and $E_x(6_1^+)/E_x(4_1^+)$. For the interacting shell model calculations, the effective charges $e_\pi = 1.31e$ and $e_\nu = 0.46e$ have been used.

The Cr isotopes have also been analyzed through Hartree-Fock/Hartree-Fock-Bogoliubov models and variations. Sato *et al.* [20] investigate the nature of the quadrupole collectivity in neutron-rich Cr isotopes $^{58-66}$Cr by using the constrained Hartree-Fock-Bogoliubov plus local quasiparticle random-phase approximation method; the calculations indicate that Cr isotopes around ^{64}Cr are prolately deformed but still have transitional character. Oba and Matsuo [21] study the deformation mechanism in neutron-rich Cr, Fe and Ti isotopes with $N = 32$–44 using a Skyrme-Hartree-Fock-Bogoliubov mean-field code; the results show a quadrupole instability around the neutron numbers $N \sim 38$–42 in Cr isotopes, indicating an onset of deformation in this neutron range.

The ^{48}Cr nucleus has been described by the $^{40}\mathrm{Ca} + \alpha + \alpha$ configuration. Descouvemont [22] applies a microscopic three-cluster model with the use of the generator coordinate method to investigate the ^{12}C, ^{24}Mg, and ^{48}Cr nuclei, described by $\alpha+\alpha+\alpha$, $^{16}\mathrm{O}+\alpha+\alpha$ and $^{40}\mathrm{Ca}+\alpha+\alpha$ configurations, respectively. Concerning ^{48}Cr, reasonable $B(E2)$ values are obtained without effective charges, the ground state band is obtained in good agreement with experimental levels, and excited bands are predicted. Sakuda and Ohkubo [23] analyze ^{48}Cr by using the $^{40}\mathrm{Ca} + \alpha + \alpha$ orthogonality condition model; the energy spectra, electromagnetic transitions, and spectroscopic factors for the $\alpha + {}^{44}$Ti and $^{8}\mathrm{Be} + {}^{40}$Ca channels were calculated. Good agreement with the experimental data is obtained for the energy spectra and $B(E2)$ transition rates, and exotic 2α-cluster states are predicted.

The α-transfer reactions are viewed as experimental means for the identification of α-cluster states. The $(^6\mathrm{Li}, d)$ and $(^{16}\mathrm{O}, {}^{12}\mathrm{C})$ reactions were used in experimental works for spectroscopic analyses of Cr isotopes. Faraggi *et al.* [24] performed the $(^{16}\mathrm{O}, {}^{12}\mathrm{C})$ reaction on several Ca and Ti target isotopes using 40 and 48 MeV ^{16}O beams. Several ^{52}Cr and ^{54}Cr energy levels are populated in the $^{48}\mathrm{Ti}(^{16}\mathrm{O},{}^{12}\mathrm{C})^{52}\mathrm{Cr}$ and $^{50}\mathrm{Ti}(^{16}\mathrm{O},{}^{12}\mathrm{C})^{54}\mathrm{Cr}$ reactions, respectively, and there is a strong selective excitation of states between 4 and 10 MeV. Fulbright *et al.* [25] performed the $(^6\mathrm{Li}, d)$ reaction on doubly even fp-shell targets using 28–38 MeV ^{6}Li beams. Energy levels of ^{54}Cr below 3.5 MeV are populated and identified through the $^{50}\mathrm{Ti}(^6\mathrm{Li}, d)^{54}\mathrm{Cr}$ reaction. A DWBA analysis of the angular distributions is made to deduce the spins and parities of some ^{54}Cr levels.

The nuclei of the Cr region have been intensively studied in recent years, since changes in the nuclear shell structure have been observed with the increase of neutron number in the isotopic chain, raising a question about the persistence of the traditional magic numbers in neutron-rich nuclei of the fp-shell. A subshell closure at $N = 32$ is indicated by new measurements of nuclear masses, high 2_1^+ energy levels, and low $B(E2; 0_1^+ \rightarrow 2_1^+)$ values in nuclei as ^{52}Ca [26,27], ^{54}Ti [28,29], and ^{56}Cr [30,31] compared with neighboring isotopes, and a subshell closure at $N = 34$ has been observed in ^{54}Ca [32]. Different studies [18,19,33,34] aim for an increase of collectivity for neutron-rich nuclei in the fp-shell region near $N = 40$. In this context, the present work contributes to further discussions on the nuclear structure of this region.

The next section describes a criterion for selection of the preferential nuclei for α-clustering in the set of even-even Cr isotopes. In sect. 3, the α-cluster model and $\alpha +$ core potential are described in detail. In sect. 4, an analysis of the selected nuclei (^{46}Cr and ^{54}Cr) is presented from the standpoint of the LPM. Conclusions are shown in sect. 5.

2 Selection of preferential nuclei for α-clustering

This paragraph describes a criterion to determine the most favorable nuclei for α-clustering in a specified set of nuclei. The criterion is the same employed in our previous work [5] for intermediate mass nuclei. An appropriate quantity for comparing different nuclei is the variation of average binding energy per nucleon of the system due to the $\alpha +$ core decomposition, given by

$$\frac{Q_\alpha}{A_T} = \frac{B_\alpha + B_{\mathrm{core}} - B_T}{A_T}\,, \tag{1}$$

where Q_α is the Q-value for α-separation, A_T is the mass number of the total nucleus and B_α, B_{core} and B_T are the binding energies of the α-cluster, the core and the total nucleus, respectively. The most favorable system (total nucleus) for α-clustering is considered to be the one with the greatest increase (or smallest decrease) in its binding energy per nucleon resulting from the separation of α-cluster and core. This criterion takes into account naturally the possible effects of closed shells (or subshells) in the core and total nucleus, since it is based on binding energies determined from experimental data [35,36]. Thus, an absolute (or local) maximum of Q_α/A_T indicates the preferred nucleus for α-clustering in comparison with the rest of (or neighbouring) nuclei in the set.

The selection process focuses mainly on the comparison of Cr isotopes, with an additional analysis of related isobaric chains. Figure 1 shows graphically the values of Q_α/A_T for even-even Cr isotopes, where there are

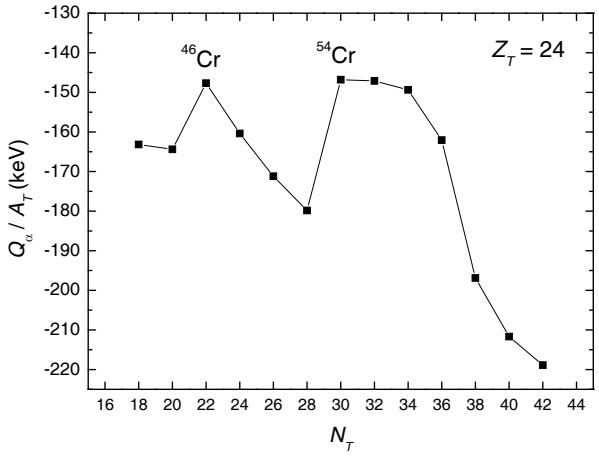

Fig. 1. Q_α/A_T values obtained for the $\alpha+$core decomposition of even-even Cr isotopes as a function of the total neutron number N_T. The Q_α/A_T peaks corresponding to ^{46}Cr and ^{54}Cr are indicated.

two Q_α/A_T peaks for ^{46}Cr (≈ -147.7 keV) and ^{54}Cr (≈ -146.8 keV). These nuclei correspond to ^{42}Ti and ^{50}Ti cores with magic numbers of neutrons $N = 20$ and $N = 28$, respectively. However, the ^{56}Cr and ^{58}Cr isotopes have Q_α/A_T values (≈ -147.1 keV and -149.4 keV, respectively) very close to those of ^{46}Cr and ^{54}Cr. This feature suggests the influence of a neutron subshell closure above $N = 28$ for the core. In the case of ^{58}Cr, there is a ^{54}Ti core with $N_{\rm core} = 32$, which is related to a subshell closure as discussed in previous studies (see sect. 1).

Figure 2 shows graphically the values of Q_α/A_T for even-even $A = 46, 54, 56, 58$ isobars. An absolute Q_α/A_T peak is seen to ^{46}Cr in the $A = 46$ graph, and a local peak is seen for ^{54}Cr in the $A = 54$ graph. However, the ^{56}Cr and ^{58}Cr nuclei do not correspond to absolute or local maxima of Q_α/A_T in the $A = 56$ and $A = 58$ graphs. Therefore, an overall evaluation of the Q_α/A_T values in figs. 1 and 2 implies that ^{46}Cr and ^{54}Cr are preferential nuclei for α-clustering if they are compared with other even-even Cr isotopes and respective even-even isobars simultaneously. These two Cr isotopes are then selected for a more detailed study in next sections.

The existence of two Q_α/A_T peaks with very close values in fig. 1 indicates a transition from $N_{\rm core} = 20$ to $N_{\rm core} = 28$ as two preferential numbers for α-clustering in this mass region. However, the variation of Q_α/A_T is influenced by the changes in the nuclear shell structure for neutron-rich nuclei, and also the liquid drop behavior of the binding energy which is significant for many nuclei. For this reason, in other isotopic chains, the preferential number of neutrons for the core may vary in relation to the traditional magic numbers.

3 α-cluster model

The properties of the nucleus are analyzed in terms of a preformed α-particle orbiting an inert core. Internal excitations of the α-cluster and the core are not considered in

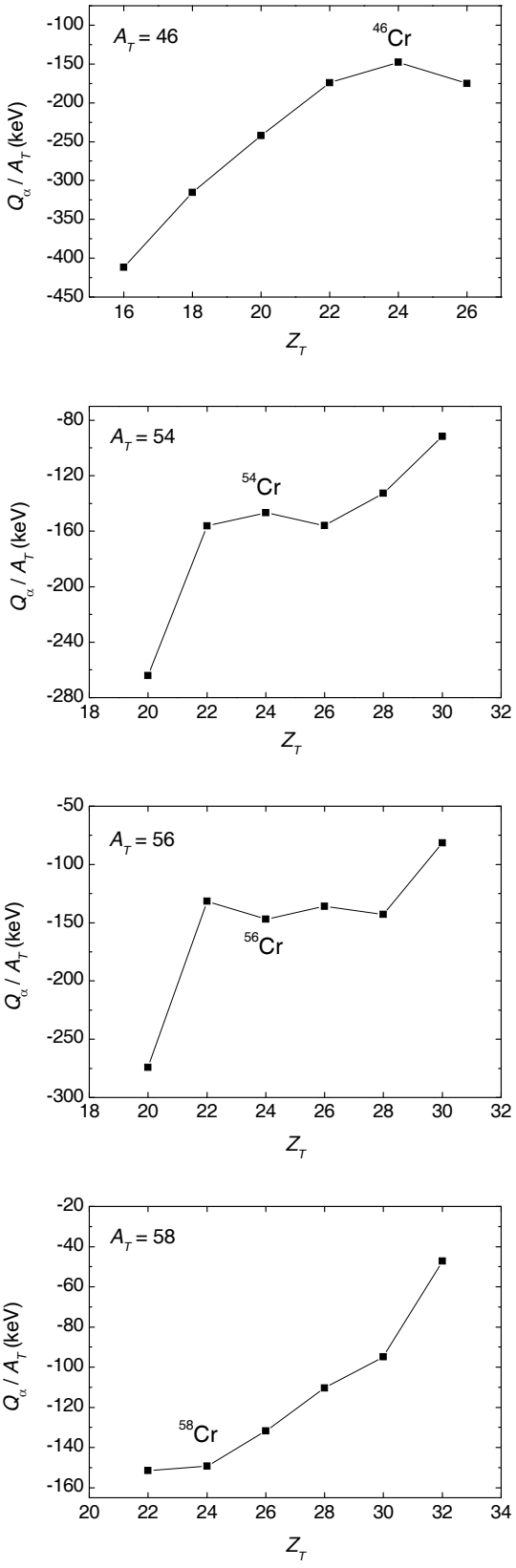

Fig. 2. Q_α/A_T values obtained for the $\alpha+$core decomposition of even-even $A = 46, 54, 56, 58$ isobars as a function of the total charge number Z_T. The Q_α/A_T values corresponding to ^{46}Cr, ^{54}Cr, ^{56}Cr, and ^{58}Cr are indicated.

Table 1. Values of the parameters R and σ for ^{46}Cr and ^{54}Cr.

Nucleus	System	R (fm)	σ (fm)
^{46}Cr	$\alpha + {}^{42}$Ti	4.658	0.248
^{54}Cr	$\alpha + {}^{50}$Ti	4.674	0.210

the calculations. The α + core interaction is described by a local phenomenological potential $V(r) = V_N(r) + V_C(r)$ containing the nuclear and Coulomb terms. For the nuclear potential, we adopt the form

$$V_N(r) = -V_0 \left[1 + \lambda \exp\left(-\frac{r^2}{\sigma^2}\right)\right] \left\{\frac{b}{1+\exp[(r-R)/a]} + \frac{1-b}{\{1+\exp[(r-R)/3a]\}^3}\right\}, \quad (2)$$

where R and σ are free parameters and V_0, λ, a, and b are fixed parameters. The Coulomb potential $V_C(r)$ is taken to be that of an uniform spherical charge distribution of radius $R_C = R$.

The shape employed in eq. (2) is a variation of the modified Woods-Saxon potential W.S. + W.S.^{3}. The W.S.+W.S.^{3} shape was originally proposed by Buck, Merchant and Perez [7] for the study of α-cluster states in the nuclei ^{20}Ne, ^{44}Ti, ^{94}Mo, and ^{212}Po; such a shape was more suitable to describe the ground state bands of the four cited nuclei and the α-decay half-lives in many heavy nuclei, compared to other traditional nuclear potential forms. Moreover, the W.S. + W.S.^{3} form was successfully applied for the investigation of the α-cluster structure in intermediate mass nuclei around ^{94}Mo [5]. In the present work, we include the factor of type (1 + Gaussian) in the nuclear potential, since it allows the correct reproduction of the 0^+ bandhead which is described roughly with the original W.S. + W.S.^{3} potential in previous calculations for other nuclei [5,7].

The ground state bands of ^{46}Cr and ^{54}Cr are calculated with the fixed values $V_0 = 220$ MeV, $a = 0.65$ fm, $b = 0.3$, and $\lambda = 0.14$, while R and σ are adjusted separately for each nucleus. The values of V_0, a and b are the same used in refs. [5,7] to describe the ground state bands of nuclei of different mass regions with the W.S. + W.S.^{3} nuclear potential. The value of λ is fitted previously to reproduce the 0^+ bandheads of the ground state bands of ^{20}Ne, ^{44}Ti, ^{94}Mo, and ^{212}Po, taking the corresponding R values obtained from ref. [5]. Then, by using the fixed values of V_0, a, b, and λ, the parameters σ and R are fitted to reproduce the experimental 0^+ and 4^+ members of the ground state bands of ^{46}Cr and ^{54}Cr (see table 1).

The Pauli principle requirements for the α valence nucleons are introduced through the quantum number

$$G = 2N + L, \quad (3)$$

where N is the number of internal nodes in the radial wave function and L is the orbital angular momentum. In this way, the restriction $G \geq G_{\text{g.s.}}$ is applied, where $G_{\text{g.s.}}$ corresponds to the ground state band. The value $G_{\text{g.s.}} = 12$ is employed for ^{46}Cr and ^{54}Cr. This value is obtained from the Wildermuth condition [37] considering the $(fp)^4$ configuration.

The energy levels and respective radial wave functions are calculated by solving the Schrödinger radial equation for the reduced mass of the α + core system.

4 Results

Using the α + core potential described in sect. 3, we have calculated the ground state bands for ^{46}Cr and ^{54}Cr. The results are compared with the corresponding experimental energies in fig. 3. The figure also shows the ground state bands calculated with the simple W.S.+W.S.^{3} nuclear potential to demonstrate the influence of the (1 + Gaussian) factor on the spectra. The effect of the (1 + Gaussian) factor for $L > 0$ is very weak; therefore, only the 0^+ bandheads are changed significantly in comparison with the spectra produced by the simple W.S. + W.S.^{3} potential.

The theoretical bands obtained with the (1 + Gaussian) × (W.S. + W.S.^{3}) potential give a very good description of the experimental levels of ^{46}Cr from 0^+ to 10^+ and ^{54}Cr from 0^+ to 8^+ (uncertain assignments are indicated in fig. 3), and a reasonable description of the higher spin levels, if we consider that the fixed parameters V_0, a, b and λ have been adjusted to reproduce the spectra of nuclei of different mass regions. It is gratifying that the mentioned results are obtained without a dependence on quantum number L in the α + core potential.

According to refs. [24,25,38], the experimental 0^+, 2^+ and 4^+ levels of the ^{54}Cr g.s. band are populated in the ^{50}Ti(^{6}Li, d)^{54}Cr and ^{50}Ti(^{16}O,^{12} C)^{54}Cr reactions. Such α-transfer information reinforces the choice of these states for comparison with the calculated band. However, there is no mention that the other band members are populated in the same reactions. New α-transfer experiments may be useful to confirm the spins and parities of the levels above 6^+ and verify if the levels above 4^+ are populated by these processes. It is important to observe that there are several experimental ^{54}Cr levels above $E_x \approx 4.5$ MeV which are populated in the ^{50}Ti(^{16}O,^{12} C)^{54}Cr reaction and do not have definite assignments.

It is interesting to compare the α + core potential of this work with optical potentials used previously to describe α elastic scattering. The comparison may be done through the volume integral per nucleon pair (J_R) and root-mean-square radius ($r_{\text{rms},R}$) associated with the nuclear potential $V_N(r)$. Table 2 shows the J_R and $r_{\text{rms},R}$ values calculated for the nuclear α + core potentials of ^{46}Cr and ^{54}Cr.

Reference [41] analyzes the α-particle elastic scattering at 140 MeV on ^{50}Ti using a double folding nuclear potential with DDM3Y interaction and three different shapes for the imaginary part of the optical potential; for this case, the values $J_R = 286$–290 MeV fm^3 and $r_{\text{rms},R} = 4.482$ fm have been obtained. The J_R and $r_{\text{rms},R}$ values obtained in the present work for ^{54}Cr are close to the ones mentioned previously. The J_R and $r_{\text{rms},R}$ values

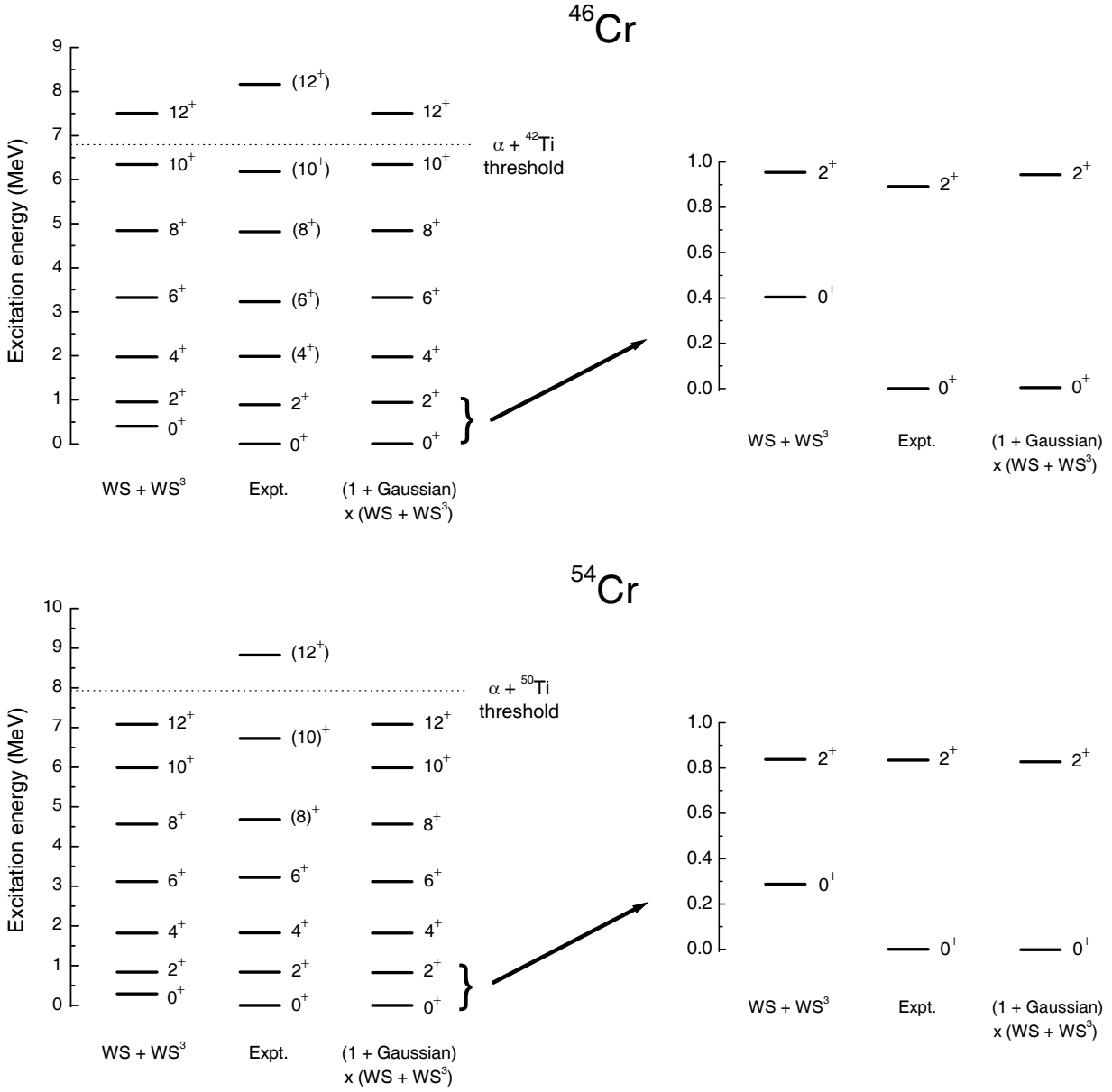

Fig. 3. Calculated α + core energies for the ground state bands of ^{46}Cr and ^{54}Cr in comparison with experimental excitation energies. The calculated g.s. bands are obtained with the W.S. + W.S.^{3} and (1 + Gaussian) × (W.S. + W.S.^{3}) nuclear potential forms, using the parameters mentioned in sect. 3. In addition, the calculated and experimental 0^+ and 2^+ levels are shown in a reduced energy scale to emphasize the effect of the (1 + Gaussian) factor for the reproduction of the 0^+ bandheads. The experimental data are from refs. [39,40,38].

of table 2 are also compatible with the ranges obtained for the same quantities in the analysis of the α elastic scattering on ^{40}Ca at different $E_{\alpha,\mathrm{lab}}$ energies [42].

It is known that J_R varies considerably with the α + core scattering energy. *E.g.*, the work of Atzrott *et al.* [42] investigates the α elastic scattering data on many target nuclei from ^{40}Ca up to ^{208}Pb over a wide range of energies, showing a decreasing trend of the volume integral with increasing α+core scattering energy, and a very small relative variation of $r_{\mathrm{rms},R}$ with the α+core scattering energy. Therefore, the comparison of the $J_R(^{54}\mathrm{Cr})$ value of this work with those of ref. [41] should not be seen as complete. However, the proximity of the calculated $J_R(^{54}\mathrm{Cr})$ and $r_{\mathrm{rms},R}(^{54}\mathrm{Cr})$ values with those of ref. [41] shows there is no discrepancy between the α + core potential applied in this work and the real part of the optical potential of ref. [41].

The radial wave functions of the states have been determined to investigate the properties discussed below. A bound state approximation has been used to calculate the radial wave functions of the states above the α + core threshold. For the calculation of the functions, the depth V_0 is adjusted smoothly for each state in order to reproduce the experimental excitation energies. It must be men-

Table 2. Calculated values of the volume integral per nucleon pair (J_R) and root-mean-square radius ($r_{\mathrm{rms},R}$) for the α+core nuclear potentials employed for ^{46}Cr and ^{54}Cr.

Nucleus	System	J_R (MeV fm^3)	$r_{\mathrm{rms},R}$ (fm)
^{46}Cr	$\alpha + {}^{42}$Ti	355.0	4.314
^{54}Cr	$\alpha + {}^{50}$Ti	301.1	4.323

Table 3. Calculated values for the rms intercluster separation ($\langle R^2\rangle^{1/2}$), the reduced α-width (γ_α^2), the dimensionless reduced α-width (θ_α^2), and the ratio of γ_α^2 to the reduced α-width $\gamma_{\alpha\,\mathrm{Ti}}^2$ calculated by Souza [47] for the corresponding J^π state in ^{44}Ti. The channel radii used for the calculation of γ_α^2 and θ_α^2 are obtained from eq. (5).

^{46}Cr ($\alpha + {}^{42}$Ti system)

J^π	$\langle R^2\rangle^{1/2}$ (fm)	γ_α^2 (keV)	θ_α^2 (10^{-3})	$\gamma_\alpha^2/\gamma_{\alpha\,\mathrm{Ti}}^2$ (%)
0^+	4.339	2.179	6.916	50.3
2^+	4.341	2.213	7.024	48.1
4^+	4.299	1.690	5.364	44.7
6^+	4.219	0.935	2.967	41.7
8^+	4.121	0.374	1.189	33.4
10^+	4.010	0.084	0.268	38.2
12^+	3.933	0.010	0.032	50.0

^{54}Cr ($\alpha + {}^{50}$Ti system)

J^π	$\langle R^2\rangle^{1/2}$ (fm)	γ_α^2 (keV)	θ_α^2 (10^{-3})	$\gamma_\alpha^2/\gamma_{\alpha\,\mathrm{Ti}}^2$ (%)
0^+	4.290	0.631	2.184	14.6
2^+	4.290	0.637	2.205	13.8
4^+	4.249	0.471	1.630	12.5
6^+	4.181	0.268	0.927	12.0
8^+	4.089	0.101	0.350	9.0
10^+	4.003	0.027	0.092	12.3
12^+	3.933	0.003	0.011	15.0

tioned that the relative variation of V_0 is below 0.15% for the states from 0^+ to 8^+, and above 1% only for the 12^+ state of ^{54}Cr.

The root-mean-square (rms) intercluster separations ($\langle R^2\rangle^{1/2}$) calculated for the g.s. bands are shown in table 3. The value of $\langle R^2\rangle^{1/2}$ is seen to decrease when one goes from the 0^+ state to the highest spin state of each band. This antistretching effect is found in nuclei of other mass regions where the α-cluster structure is studied, considering different local potential forms [5,6,43,44]. Such a result shows that the inclusion of the (1+Gaussian) factor in the nuclear potential does not significantly change this property in relation to the simple W.S. + W.S.^{3} potential.

The radial wave functions are used for the calculation of the reduced α-width [45,46]

$$\gamma_\alpha^2 = \left(\frac{\hbar^2}{2\mu a_c}\right) u^2(a_c) \left[\int_0^{a_c} |u(r)|^2 \mathrm{d}r\right]^{-1}, \qquad (4)$$

where μ is the reduced mass of the system, $u(r)$ is the radial wave function of the state and a_c is the channel radius. A procedure that avoids an arbitrary choice of the channel radius is used. The value of a_c is given by the relation [5]

$$a_c = 1.295\left(A_\alpha^{1/3} + A_{\mathrm{core}}^{1/3}\right) + 0.824\,(\mathrm{fm}), \qquad (5)$$

obtained from a linear fit that considers other channel radii used for different α + core systems in the literature. The dimensionless reduced α-width θ_α^2 is defined as the ratio of γ_α^2 to the Wigner limit, that is,

$$\theta_\alpha^2 = \frac{2\mu a_c^2}{3\hbar^2}\gamma_\alpha^2. \qquad (6)$$

The g.s. bands of ^{46}Cr and ^{54}Cr show a rapid decrease of γ_α^2 with the increasing spin (see table 3). In agreement with the analysis of the rms intercluster separations, the behavior of γ_α^2 indicates a stronger α-cluster character for the low-spin members of these bands. For the two nuclei, the dimensionless reduced α-widths θ_α^2 present a small fraction of the Wigner limit, even for the low-spin members of the band. This is an expected feature for strongly bound α+core states, or states above the α+core threshold and far below the top of the Coulomb barrier.

Table 3 also shows the ratio $\gamma_\alpha^2/\gamma_{\alpha\,\mathrm{Ti}}^2$ for each J^π state, where $\gamma_{\alpha\,\mathrm{Ti}}^2$ is the reduced α-width calculated for a corresponding J^π state of the ^{44}Ti ground state band. Such a comparison is useful since ^{44}Ti is regarded as the most favorable nucleus for the α+core structure at the beginning of the fp-shell. The $\gamma_{\alpha\,\mathrm{Ti}}^2$ values are taken from the work of Souza [47], where the reduced α-widths are calculated with the W.S.+W.S.^{3} shape for the α+core nuclear potential, and the channel radius is also determined with eq. (5). The ratio $\gamma_\alpha^2/\gamma_{\alpha\,\mathrm{Ti}}^2$ ranges from 33.4% to 50.3% for ^{46}Cr, and from 9.0% to 15.0% for ^{54}Cr. These results indicate that the α-cluster intensity for the two Cr isotopes is lower than for ^{44}Ti; however, it is revealed that the ^{46}Cr ground state band presents an expressive degree of α-clustering in comparison with ^{44}Ti. For ^{54}Cr, the $\gamma_\alpha^2/\gamma_{\alpha\,\mathrm{Ti}}^2$ ratios are smaller, but still relevant.

It is noted that the θ_α^2 values for ^{46}Cr are $\approx 3\times$ higher than the respective values for ^{54}Cr. The energy location of the α + core threshold has an important influence on this difference. In the excitation energy scale, the α+core threshold for ^{54}Cr is $\approx$ 1.1 MeV higher than the corresponding threshold for ^{46}Cr. Thus, the radial wave functions of the ^{54}Cr states are less intense in the surface region, which contributes to a lower degree of α-clustering in comparison with ^{46}Cr.

The calculated $B(E2)$ transition rates for the g.s. bands of ^{46}Cr and ^{54}Cr are presented in table 4. The formulae used to determine the $B(E2)$ values are detailed in ref. [5]. A comparison of the calculated values and experimental data shows that the model can provide the correct order of magnitude of the experimental $B(E2)$ values without the use of effective charges. These results may be considered satisfactory since, in shell-model calculations for nuclei of this mass region [18,19,49,50], substantial

Table 4. Comparison of the calculated $B(E2)$ transition rates for the ground state bands of ^{46}Cr and ^{54}Cr with the corresponding experimental data [38,48]. The calculated values have been obtained without effective charges.

^{46}Cr ($\alpha + {}^{42}$Ti system)

J^π	$B(E2; J \to J-2)$ (W.u.)	$B(E2)_{\rm exp.}$ (W.u.)
2^+	9.657	19(4)[(a)]
4^+	13.045	–
6^+	12.454	–
8^+	10.281	–
10^+	7.057	–
12^+	3.669	–

^{54}Cr ($\alpha + {}^{50}$Ti system)

J^π	$B(E2; J \to J-2)$ (W.u.)	$B(E2)_{\rm exp.}$ (W.u.)
2^+	7.456	14.4(6)
4^+	10.049	26(9)
6^+	9.688	18(5)
8^+	8.004	12.8(17)
10^+	5.729	–
12^+	2.966	–

[(a)] Deduced from the experimental $B(E2; 0^+_{\rm g.s.} \to 2^+_1)$ value obtained by K. Yamada *et al.* [48].

effective charges are necessary to reproduce the experimental data. Furthermore, it is shown that the calculated $B(E2)$ values for ^{54}Cr reproduce nicely the increasing or decreasing trend of the experimental data between the $2^+ \to 0^+$ and $8^+ \to 6^+$ transitions.

There are few negative parity levels with definite assignments for ^{46}Cr and ^{54}Cr, and the clear identification of negative parity bands is not possible. Nevertheless, we have calculated the 3^- level of the $G = 13$ band for a comparison with experimental energy levels of the two nuclei, applying the depth $V_0 = 238$ MeV which was suitable for the calculation of the negative parity bands of even-even nuclei around ^{94}Mo with the simple W.S. + W.S.^{3} potential [5]. The energies $E_{x\,\rm calc}(3^-) = 3.444$ MeV and 3.258 MeV are obtained for ^{46}Cr and ^{54}Cr, respectively, to be compared with the experimental excitation energies 3.1965 MeV (3^-_1 state, uncertain assignment) and 4.12705 MeV (3^-_1 state, definite assignment), respectively. A consistent analysis of the α+core negative parity bands depends on further experimental data.

5 Conclusions

The calculation of Q_α/A_T values for even-even Cr isotopes and even-even $A = 46, 54, 56, 58$ isobars indicates that ^{46}Cr and ^{54}Cr are the preferential nuclei for α-clustering when compared with their even-even isotopes and isobars simultaneously. The α-cluster model gives a good account of the experimental ground state bands of these two nuclei through a local α + core potential with two variable parameters. The nuclear potential with (1 + Gaussian) × (W.S. + W.S.^{3}) shape allows the correct reproduction of the 0^+ bandheads and, additionally, describes the experimental higher spin levels of the two nuclei very well using a fixed set of four parameters which was successful in describing the ground state bands in nuclei of different mass regions.

The calculations of the volume integral per nucleon pair and rms radius show that the values obtained for the ^{54}Cr nuclear potential are close to those reported for the real part of the optical potential for α-^{50}Ti elastic scattering at 140 MeV [41]. As the volume integral may vary with the α+core scattering energy, this comparison should not be seen as complete; however, it is shown that there is no discrepancy between the α-^{50}Ti optical potential and the α + core potential of this work.

The $B(E2)$ values obtained for ^{46}Cr and ^{54}Cr give the correct order of magnitude of the available experimental data without effective charges. The calculated intercluster rms radii and reduced α-widths suggest that the α-cluster character is stronger for the low-spin members of the ground state bands of ^{46}Cr and ^{54}Cr. Therefore, the use of the (1 + Gaussian) factor in the α + core nuclear potential does not change significantly this feature as compared to previous α + core calculations in different mass regions.

The comparison of the reduced α-widths for ^{46}Cr and ^{54}Cr with the respective values obtained previously for ^{44}Ti [47] indicates that the two Cr isotopes have a lower α-cluster intensity relative to ^{44}Ti. In addition, the same comparison points out that the ^{46}Cr g.s. band has an expressive degree of α-clustering compared to the ^{44}Ti g.s. band.

New experimental data, especially from α-transfer reactions, will be important to complement the analysis of this work. This study should be extended to other isotopic chains of the same region in next works.

The authors thank the members of the Nuclear Spectroscopy with Light Ions Group of University of São Paulo for the fruitful discussions. This work was financially supported by Coordenação de Aperfeiçoamento de Pessoal de Nível Superior (CAPES). Research developed with the HPC resources provided by the Information Technology Superintendence of University of São Paulo.

References

1. H. Horiuchi, K. Ikeda, K. Katō, Prog. Theor. Phys. Suppl. **192**, 1 (2012).
2. C. Beck, J. Phys. Conf. Ser. **569**, 012002 (2014).
3. B. Buck, A.C. Merchant, S.M. Perez, Few-Body Syst. **29**, 53 (2000).
4. B. Buck, A.C. Merchant, S.M. Perez, Nucl. Phys. A **657**, 267 (1999).
5. M.A. Souza, H. Miyake, Phys. Rev. C **91**, 034320 (2015).

6. F. Michel, G. Reidemeister, S. Ohkubo, Phys. Rev. C **37**, 292 (1988).
7. B. Buck, A.C. Merchant, S.M. Perez, Phys. Rev. C **51**, 559 (1995).
8. A.C. Merchant, K.F. Pál, P.E. Hodgson, J. Phys. G: Nucl. Part. Phys. **15**, 601 (1989).
9. S. Ohkubo, Y. Hirabayashi, T. Sakuda, Phys. Rev. C **57**, 2760 (1998).
10. F. Michel, S. Ohkubo, G. Reidemeister, Prog. Theor. Phys. Suppl. **132**, 7 (1998).
11. M. Kimura, H. Horiuchi, Nucl. Phys. A **767**, 58 (2006).
12. A.C. Merchant, J. Phys. G: Nucl. Phys. **10**, 885 (1984).
13. A.C. Merchant, Phys. Rev. C **36**, 778 (1987).
14. T. Sakuda, S. Ohkubo, Phys. Rev. C **51**, 586 (1995).
15. T. Sakuda, S. Ohkubo, Phys. Rev. C **57**, 1184 (1998).
16. Y. Taniguchi, Prog. Theor. Exp. Phys. **2014**, 073D01 (2014).
17. T. Togashi, N. Shimizu, Y. Utsuno, T. Otsuka, M. Honma, Phys. Rev. C **91**, 024320 (2015).
18. K. Kaneko, Y. Sun, M. Hasegawa, T. Mizusaki, Phys. Rev. C **78**, 064312 (2008).
19. J. Kotila, S.M. Lenzi, Phys. Rev. C **89**, 064304 (2014).
20. K. Sato, N. Hinohara, K. Yoshida, T. Nakatsukasa, M. Matsuo, K. Matsuyanagi, Phys. Rev. C **86**, 024316 (2012).
21. H. Oba, M. Matsuo, Prog. Theor. Phys. **120**, 143 (2008).
22. P. Descouvemont, Nucl. Phys. A **709**, 275 (2002).
23. T. Sakuda, S. Ohkubo, Nucl. Phys. A **712**, 59 (2002).
24. H. Faraggi, M.-C. Lemaire, J.-M. Loiseaux, M.C. Mermaz, A. Papineau, Phys. Rev. C **4**, 1375 (1971).
25. H.W. Fulbright *et al.*, Nucl. Phys. A **284**, 329 (1977).
26. F. Wienholtz *et al.*, Nature **498**, 346 (2013).
27. A. Gade *et al.*, Phys. Rev. C **74**, 021302(R) (2006).
28. R.V.F. Janssens *et al.*, Phys. Lett. B **546**, 55 (2002).
29. D.-C. Dinca *et al.*, Phys. Rev. C **71**, 041302(R) (2005).
30. A. Bürger *et al.*, Phys. Lett. B **622**, 29 (2005).
31. J.I. Prisciandaro *et al.*, Phys. Lett. B **510**, 17 (2001).
32. D. Steppenbeck *et al.*, Nature **502**, 207 (2013).
33. C.F. Jiao, J.C. Pei, F.R. Xu, Phys. Rev. C **90**, 054314 (2014).
34. H.L. Crawford *et al.*, Phys. Rev. Lett. **110**, 242701 (2013).
35. G. Audi, M. Wang, A.H. Wapstra, F.G. Kondev, M. MacCormick, X. Xu, B. Pfeiffer, Chin. Phys. C **36**, 1287 (2012), `http://amdc.in2p3.fr/web/masseval.html`.
36. M. Wang, G. Audi, A.H. Wapstra, F.G. Kondev, M. MacCormick, X. Xu, B. Pfeiffer, Chin. Phys. C **36**, 1603 (2012), `http://amdc.in2p3.fr/web/masseval.html`.
37. K. Wildermuth, Y.C. Tang, *A Unified Theory of the Nucleus* (Academic Press, New York, 1977).
38. Yang Dong, Huo Junde, Nucl. Data Sheets **121**, 1 (2014).
39. Balraj Singh, *ENSDF* Database, `http://www.nndc.bnl.gov/ensdf/`.
40. S.-C. Wu, Nucl. Data Sheets **91**, 1 (2000).
41. A.M. Kobos, B.A. Brown, P.E. Hodgson, G.R. Satchler, A. Budzanowski, Nucl. Phys. A **384**, 65 (1982).
42. U. Atzrott, P. Mohr, H. Abele, C. Hillenmayer, G. Staudt, Phys. Rev. C **53**, 1336 (1996).
43. B. Buck, C.B. Dover, J.P. Vary, Phys. Rev. C **11**, 1803 (1975).
44. S. Ohkubo, Phys. Rev. Lett. **74**, 2176 (1995).
45. A. Arima, S. Yoshida, Nucl. Phys. A **219**, 475 (1974).
46. G. Michaud, L. Scherk, E. Vogt, Phys. Rev. C **1**, 864 (1970).
47. M.A. Souza, *Estrutura de Cluster-alfa em Núcleos da Região do Molibdênio*, PhD Thesis, University of São Paulo (2010) p. 74.
48. K. Yamada *et al.*, Eur. Phys. J. A **25**, 409 (2005).
49. K. Langanke, D.J. Dean, P.B. Radha, Y. Alhassid, S.E. Koonin, Phys. Rev. C **52**, 718 (1995).
50. K. Itonaga, Prog. Theor. Phys. **66**, 2103 (1981).